THE JOURNAL OF PHYSICAL CHEMISTRY A LETTERS

2005, *109,* 6628−6633
Published on Web 07/12/2005

Electronic Structure and Electron Transport Characteristics of a Cobalt Complex

Liuming Yan[†] and Jorge M. Seminario*[,†,‡]

Department of Chemical Engineering and Department of Electrical Engineering, Texas A&M University, 3122 TAMU, College Station, Texas 77843-312

Received: May 26, 2005; In Final Form: June 25, 2005

The molecular and electronic structures and electron transport characteristics of a Co complex are investigated using first principles calculations. The Co complex belongs to the D_{2d} point group, and its two ligands are perpendicular to each other. The central atom Co forms a distorted octahedron with six donor N atoms. In a low oxidation state, the bond length between Co and pyrrole nitrogen, 1.849 Å, is much shorter than the distance between Co and pyridine nitrogen, 2.168 Å, while, in a high oxidation state, the bond length differences between Co and pyrrole nitrogen, 1.814 Å, and between Co and pyridine nitrogen, 1.990 Å, are not as large as those in the Co^{2+} complex. The HOMO energy of the low oxidation state is very close to the Fermi level of bulk Au, allowing hole creation in the molecule. On the other hand, the LUMO energy of the high oxidation state is close to the Au Fermi level, allowing a low barrier for electron injection from the Au cathode to the molecule. These structural characteristics make the Co complex a good hole-conduction molecule. The density of states, transmission probability, and $I-V$ characteristics are evaluated using the Green function approach.

1. Introduction

One of the most studied groups of organic molecules in molecular electronics is conjugated organics. It has been proven both experimentally and theoretically that conjugate molecules can perform as electron conductors and switches.[1−3] However, good conductivity and switching are not enough for the fabrication of molecular electronic devices;[4−6] molecular electronic devices must have bonding ability, allowing them to interconnect with each other and to be addressed by external terminals[7] or, alternatively, to show molecular programmability characteristics to compensate for the lack of addressability.[8,9] In most of the published studies, molecules are attached to terminals via S−Au bonds, which are formed in the reaction between a thiol group (−SH) and a Au terminal.[10−12] However, the stability or rigidity of a single S−Au bond to hold the molecule to the contact is one of the major problems. Molecules with two or more thiol groups would yield more robust molecular circuits. Co complex **1** (Chart 1) is an aromatic molecule suitable for a dual S−Au bonding to each Au terminal.[13] Cobalt is a typical bivalent transition metal. Co complexes have special characteristics to function as electron transfer intermediates permitting a high electron transfer probability.[14−18] Co complex **1** can be self-assembled between two Au terminals with dual S−Au bonds on both terminals, forming molecular device **2**. The study of **2** connected to an external voltage source can be simplified by conveniently partitioning it into two semi-infinite terminals and core molecule **3** or, alternatively, two semi-infinite terminals and the extended molecule (**4**).

The molecular and electronic structures are calculated using ab initio density functional theory (DFT). The electron transmission characteristics are calculated using the Green function approach based on quantum transport theory.[19,20]

We describe the methodology in section 2; results in section 3, including the optimized geometry, electronic structure, density of states (DOS), electron transmission probability (T), and current−voltage ($I-V$) characteristics; and concluding remarks in section 4.

2. Methodology

The Hamiltonian for the molecular device, $\mathbf{H}_{\text{device}}$, consisting of a left semi-infinite Au terminal (L), a right semi-infinite Au terminal (R), and core molecule **3** can be written as

$$\mathbf{H}_{\text{device}} = \mathbf{H_3} + \mathbf{H}_{\text{L}} + \mathbf{H}_{\text{R}} + \mathbf{H}_{\text{L}\mathbf{3}} + \mathbf{H}_{\mathbf{3}\text{R}} + \mathbf{H}_{\text{LR}} \qquad (1)$$

where $\mathbf{H_3}$, $\mathbf{H}_{\text{L}}$, $\mathbf{H}_{\text{R}}$, $\mathbf{H}_{\text{L}\mathbf{3}}$, $\mathbf{H}_{\mathbf{3}\text{R}}$, and $\mathbf{H}_{\text{LR}}$ represent the Hamiltonians of the isolated core molecule, left terminal, right terminal, coupling between left terminal and core molecule, coupling between core molecule and right terminal, and coupling between left and right terminals, respectively. We use the following approach to approximate the device Hamiltonian.

The Kohn−Sham density functional theory is applied to **4**, representing the molecular wave function in contracted Gaussian type basis functions, $|\chi_j\rangle$,[21,22]

$$\mathbf{H}_4^{\text{KS}} \sum_{j=1}^{N} c_j |\chi_j\rangle = \epsilon \mathbf{S}_4 \sum_{j=1}^{N} c_j |\chi_j\rangle \qquad (2)$$

where $\mathbf{H}_4^{\text{KS}}$ is the Kohn−Sham Hamiltonian, $\mathbf{S}_4$ is the overlap matrix, ϵ are the eigenvalues, c_j are expansion coefficients, and the summation j runs over all atomic basis functions. Then, the

[†] Department of Chemical Engineering.
[‡] Department of Electrical Engineering.

10.1021/jp052798k CCC: $30.25

CHART 1: Co Complexes 1−4 and Atomic Labeling (Only Symmetrically Distinct Atoms Are Labeled)[a]

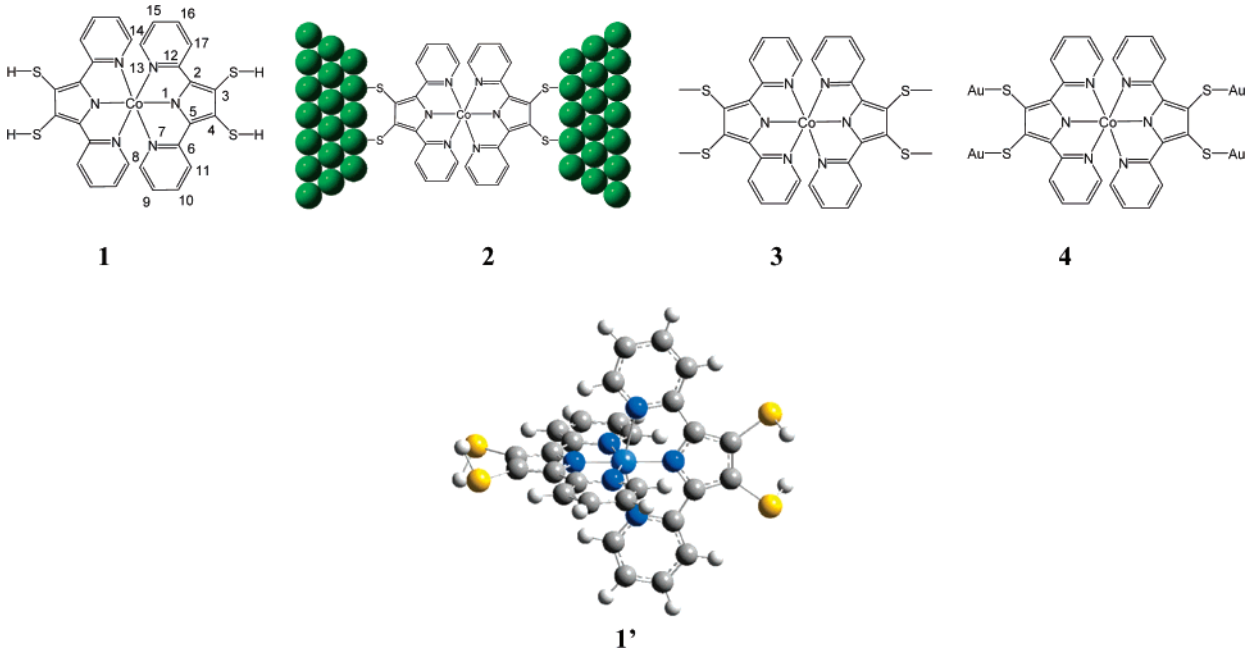

1 **2** **3** **4** **1'**

[a] **2** is **1** attached to Au terminals; atoms beyond those attached to the molecule are treated as bulk. **3** is the core molecule attached to the contacts, and **4** is the extended molecule (the Au atoms on the left and right are contacts 1 and 2, respectively). The Co atom is a typical bivalent metal; both the low oxidation state (Co^{2+}) and the high oxidation state (Co^{3+}) can exist. **1′** is the ball-and-bond representation of **1**. Notice that these molecular structures are not planar; in all cases, the left part of the molecule is perpendicular to the right one, as shown in **1′**.

Kohn−Sham Hamiltonian is transformed to

$$\mathbf{H}_4 = \mathbf{S}_4^{-1}\mathbf{H}_4^{KS} \tag{3}$$

to ensure its hermiticity.[23] The transformed Hamiltonian matrix $\mathbf{H}_4$ is then rearranged into submatrixes:[19,20]

$$\mathbf{H}_4 = \begin{bmatrix} \mathbf{H}_{11} & \mathbf{H}_{1M} & \mathbf{H}_{12} \\ \mathbf{H}_{M1} & \mathbf{H}_{MM} & \mathbf{H}_{M2} \\ \mathbf{H}_{21} & \mathbf{H}_{2M} & \mathbf{H}_{22} \end{bmatrix} \tag{4}$$

The $\mathbf{H}_{MM}$ matrix elements are $H_{lm} = \langle\chi_l|\mathbf{H}|\chi_m\rangle$, with l and m running over all basis functions centered on the core molecule; it corresponds to the Hamiltonian submatrix of the core molecule. $\mathbf{H}_{11}$ and $\mathbf{H}_{22}$ are the Hamiltonian submatrixes of the contacts. $\mathbf{H}_{M1}$ and $\mathbf{H}_{1M}$ are the Hamiltonian submatrixes of the core molecule and contact 1 interaction, $\mathbf{H}_{M2}$ and $\mathbf{H}_{2M}$ are the corresponding ones for the Hamiltonian submatrixes between core molecule and contact 2, $\mathbf{H}_{12}$ and $\mathbf{H}_{21}$ are the Hamiltonian submatrixes between contact 1 and contact 2.

Then, a self-energy term, Σ_j ($j = 1, 2$), is used to represent the effect from the terminals[24,25] using

$$\Sigma_j = \mathbf{H}_{Mj}\mathbf{g}_j(E)\mathbf{H}_{jM} \tag{5}$$

where $\mathbf{g}_j(E)$ is the Green function of the terminal.[19,20] The Green function, $\mathbf{g}_j(E)$, is defined using the local density of states—DOS$_j^k s(E)$, DOS$_j^k p(E)$, DOS$_j^k d_{e_g}(E)$, and DOS$_j^k d_{t_{2g}}(E)$—of the bulk contacts projected to the s, p, d_{e_g}, and $d_{t_{2g}}$ subshells.

$$\mathbf{g}_j^k(E) = \begin{bmatrix} \mathrm{DOS}_j^k s(E) & 0 & 0 & 0 \\ 0 & \mathrm{DOS}_j^k p(E) & 0 & 0 \\ 0 & 0 & \mathrm{DOS}_j^k d_{e_g}(E) & 0 \\ 0 & 0 & 0 & \mathrm{DOS}_j^k d_{t_{2g}}(E) \end{bmatrix} \tag{6}$$

The index k (=1, 2) runs over all of the contact atoms; thus, we have

$$\mathbf{g}_j(E) = \pi i \times \begin{bmatrix} \mathbf{g}_j^1(E) & 0 \\ 0 & \mathbf{g}_j^2(E) \end{bmatrix} \tag{7}$$

where i is the imaginary unit.

Therefore, the Hamiltonian of the device is written as

$$\mathbf{H}_{device} = \mathbf{H}_{MM} + \Sigma_1 + \Sigma_2 \tag{8}$$

and the Green function for the molecular device is evaluated as

$$\mathbf{G}_M = [E\mathbf{I} - \mathbf{H}_{device}]^{-1} \tag{9}$$

Notice that the bulk contact Green function is an input to the transport formalism. The complex nature of $\mathbf{g}_j(E)$ yields complex self-energy terms that are responsible for the broadening and shifting of the discrete molecule.

The electron transmission function and density of states of the molecular device are obtained from the Green function according to the following equations:[26]

$$T(E) = \frac{1}{N}\mathrm{tr}(\mathbf{\Gamma}_1\mathbf{G}_M\mathbf{\Gamma}_2\mathbf{G}_M^+) \tag{10}$$

$$\mathrm{DOS} = \mathrm{tr}[i(\mathbf{G}_M - \mathbf{G}_M^+)] \tag{11}$$

where $\mathbf{\Gamma}_j = i(\mathbf{\Sigma}_j - \mathbf{\Sigma}_j^+)$ ($j = 1, 2$) is the imaginary part of the self-energy, $\mathbf{\Sigma}_j$; $\mathbf{G}_M^+$ is the adjoint of $\mathbf{G}_M$; and N is the number of atomic basis functions. The current as a function of the external bias is obtained according to the Landauer−Büttiker equation:[27−29]

$$I(V) = \frac{2e}{h}\int_{-\infty}^{\infty} T(E,V)[f_1(E,V_1) - f_2(E,V_2)]\,\mathrm{d}E \tag{12}$$

TABLE 1: Structural Parameters of the Ground State of the Extended Molecule

	oxidation state of Co	
	Co^{2+}	Co^{3+}
	Bond Length (Å)	
N1−C2	1.362	1.356
C2−C3	1.423	1.424
C3−C4	1.442	1.445
C5−C6	1.452	1.449
C6−N7	1.382	1.393
N7−C8	1.348	1.350
C8−C9	1.403	1.399
C9−C10	1.407	1.407
C10−C11	1.400	1.400
C11−C6	1.409	1.405
Co−N1	1.849	1.814
Co−N7	2.168	1.990
S−Au	2.641	2.649
C−S	1.804	1.803
Au−Au	3.008	2.982
	Bond Angle (deg)	
C2−N1−C5	111.4	113.0
N1−C2−C3	107.8	106.9
C2−C3−C4	106.5	106.6
N1−C5−C6	113.2	110.2
C5−C6−N7	112.7	112.2
C6−N7−C8	119.5	120.1
N7−C8−C9	122.6	121.8
C8−C9−C10	118.4	118.8
C9−C10−C11	119.7	119.8
C10−C11−C6	119.1	119.4
C11−C6−N7	120.8	120.1
N1−Co−N7	77.3	79.8
C2−C3−S	128.0	127.6
C−S−Au	90.0	90.0

where $I(V)$ is the current, $f_j(E,V_j)$ is the Fermi function, V_1 and V_2 are the electric potentials of the terminals, e is the charge of the electron, and h is the Planck constant.

The electronic structure of the Co extended molecule is calculated using Kohn−Sham density functional theory (KS-DFT)[21,22,30] as implemented in the Gaussian 03 program[31] using the Becke three-parameter hybrid exchange functional[32] with the Perdew−Wang correlation functional (B3PW91).[33−35] The geometry optimizations are carried out progressively: the molecules are optimized within D_{2d} molecular symmetry using LANL2DZ basis sets and effective core potential (ECP);[36−38] then, a larger basis set is used—the 6-31G(d,p) basis set[39,40] for H, C, N, and S and the Stuttgart/Dresden basis set and ECP for Co[41] and Au.[42−44] Finally, the symmetry constraints are relaxed and stable structures are found using the larger basis sets. The optimization is followed by a second derivative calculation, to confirm the stability of the optimized structure.

In a coordination environment, the Co 3d orbitals split. For example, Co 3d orbitals split into triply degenerate orbitals t_{2g} and a doubly degenerate e_g. These two sets of orbitals also split in a distorted octahedral coordination environment. The occupation of these orbitals depends on the relative value of the splitting energy and the electron correlation energy; thus, a high spin state or low spin state could exist.[45] Our optimizations are carried out with all possible spin states. For the low oxidation state (Co^{2+}), the possible spin states are a quartet for high spin states and a doublet for low spin states. For the high oxidation state (Co^{3+}), the possible spin states are a quintet ($m = 5$) for high spin states, a triplet ($m = 3$), and a singlet ($m = 1$) for low spin states.

After the geometry of the extended molecule (**4**) is optimized using the Gaussian 03 program, the effect of the bias electric field on the extended molecule (**4**) is evaluated by performing a series of ab initio calculations with different electric fields applied to the extended molecule; the Hamiltonian submatrixes $\mathbf{H}_{MM}$, $\mathbf{H}_{1M}$, and $\mathbf{H}_{2M}$ corresponding to applied electric field are obtained. Then, the DOS for bulk Au is calculated using the Crystal 98 program[46] at the B3PW91/LANL2DZ[33−38] level of theory and the self-energy is calculated using eqs 5−7. Then, a series of Green functions corresponding to different applied electric fields are calculated, and finally, the density of states, electron transport probabilities, and current−voltage characteristics are calculated using the Green function. In this manner, both effects, from the terminals and from the applied electric fields, are explicitly considered in a many-body approach to electron transfer.

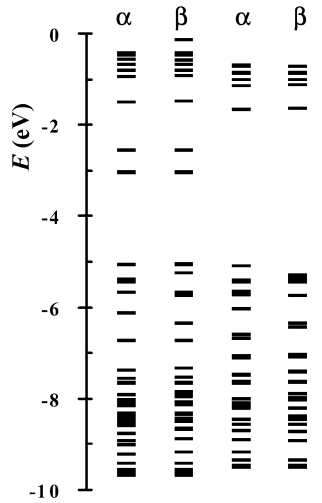

Figure 1. Energy levels of molecule **4** (first two columns of bars) and **1** (last two columns of bars). The HOMO−LUMO gap of **1** is 3.64 eV; however, four α and four β spin orbitals are inserted into the HOMO−LUMO gap when the molecule is attached to the two Au terminals, forming the extended molecule (**4**). The HOMO−LUMO gap of **4** is 1.83 eV.

3. Results, Discussions, and Conclusions

Our calculation shows that low spin states are more stable for both the high and low oxidation states for the extended molecule (**4**). For the low oxidation state, the doublet is lower than the quartet by 0.34 eV, and for high oxidation state, the singlet is 1.30 eV lower than the triplet.

The optimized structural parameters for the extended molecule are summarized in Table 1. The extended molecule has D_{2d} symmetry with two ligands perpendicular to each other. The Co and its donors, six N atoms, form a distorted octahedron. The bond length between Co and pyrrole nitrogen (N1) is shorter than the bond length between Co and pyridine nitrogen (N7 and N13). Furthermore, the four pyridine N atoms are not coplanar.

The importance of having precise and optimized structures of the extended molecule is of paramount importance in molecular electronics. A typical example from basic organic chemistry shows us that small variations of only ∼0.1 Å are enough to determine a single, double, triple, or resonant C−C bond with each of these bonds having totally different characteristics. A more crucial example of the importance of precisely determining geometries actually comes from the actual fabrication of electronic devices: To improve its electric properties, Si is grown on a substrate containing Ge; this produces strained Si, which has a Si−Si bond length of only 1% longer than the normal or unstrained Si; however, the electron mobility in strained Si is close to twice that in unstrained Si.[47]

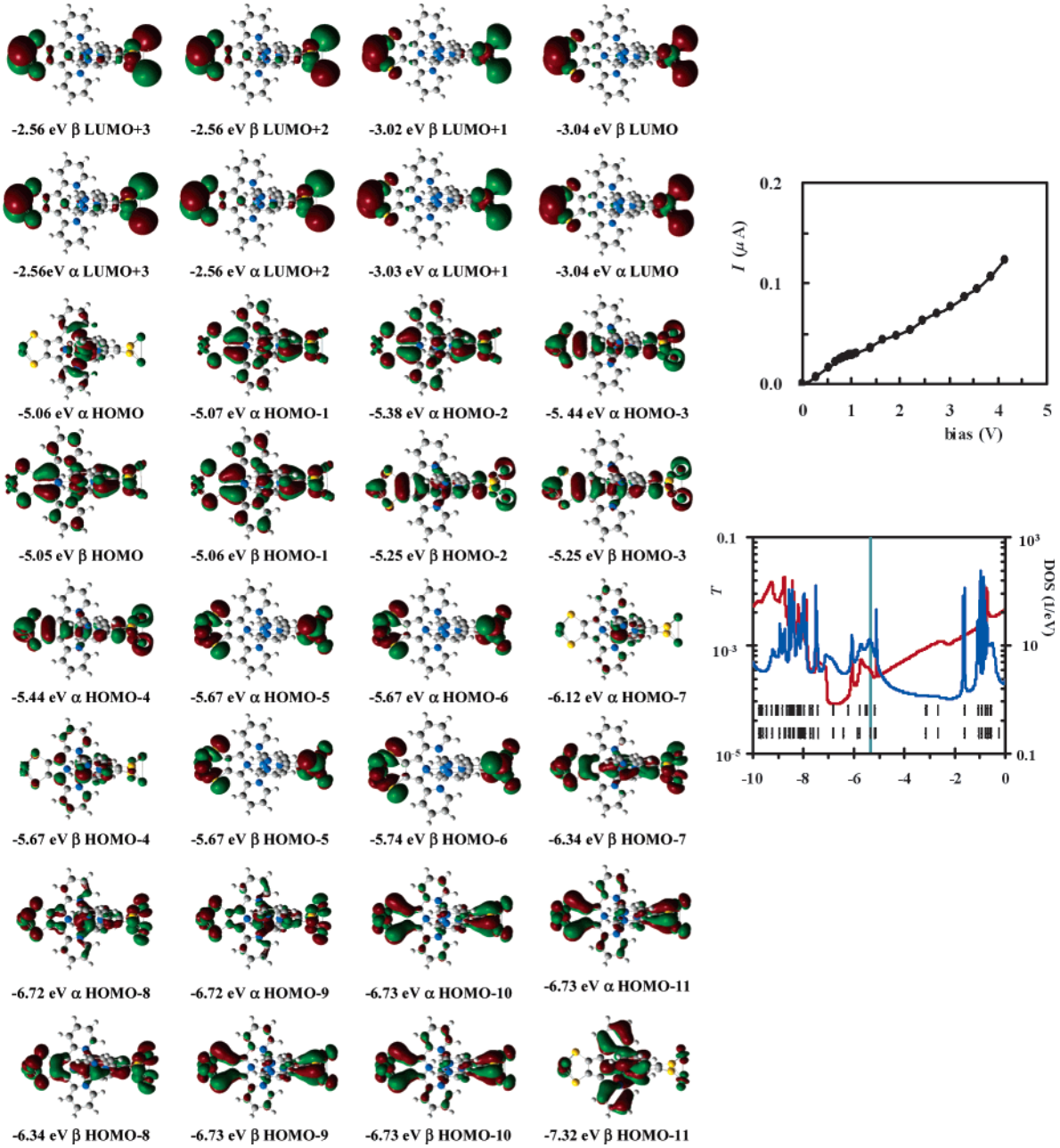

Figure 2. (left) Molecular orbital of the extended molecule (**4**) in the low oxidation state; (top right) $I-V$ characteristics; (bottom right) DOS (blue, right axis) and electron transmission probability (red, left axis) (the vertical green line represents the Au Fermi level, and the short black lines are electronic states of the extended molecule (**4**)).

The ionization potential for the extended molecule, the energy difference between the low and high oxidation states, is 5.32 eV. Due to the stronger attraction between Co^{3+} and N than that between Co^{2+} and N, the donor N atoms are closer to Co^{3+} than to Co^{2+}. The effects of oxidation on different Co−N bond lengths are different. The bond length between Co and pyridine N7 decreases from 2.168 to 1.990 Å by oxidation, while the bond length between Co and pyrrole N1 decreases from 1.849 to 1.814 Å only.

To investigate the electronic structure and electron transmission of the molecular device at the low oxidation state, we notice that the HOMO−LUMO gap of **1** is 3.64 eV; however, the reaction of **1** with Au causes the HOMO−LUMO gap to decrease to 1.83 eV in **4**. **4** has similar MOs to those of **1**, except for the extra MOs related to Au. For example, eight extra unoccupied spin MOs (α-LUMO to α-LUMO+3 and β-LUMO to β-LUMO+3) exist in the HOMO−LUMO gap of **1** (Figure 1).

For an isolated molecule, the Hamiltonian operator is Hermitian, and its eigenvalues are real. However, the device Hamiltonian matrix, $\mathbf{H}_{\text{device}}$ (eq 8), is not Hermitian; the imaginary self-energy terms that depend on the terminal Green function cause the shift and broadening of the eigenvalues. For molecular devices, there are three groups of peaks on the DOS corresponding to three groups of MOs of the extended molecule (**4**). The peaks near the Fermi level correspond to HOMO to HOMO−10 (Figure 2). The contribution of different MOs of **4** to the DOS of the device is not the same. A delocalized MO contributes more to the DOS than a localized one; thus, a delocalized MO yields a peak in the DOS curve.

A delocalized MO also contributes more to the transmission probabilities in the molecular device. For molecule **4**, the α-HOMO is localized on the Co coordination bonds. Below α-HOMO, there are eight delocalized MOs (α-HOMO−1 to α-HOMO−4 and β-HOMO to β-HOMO-3), and their orbital

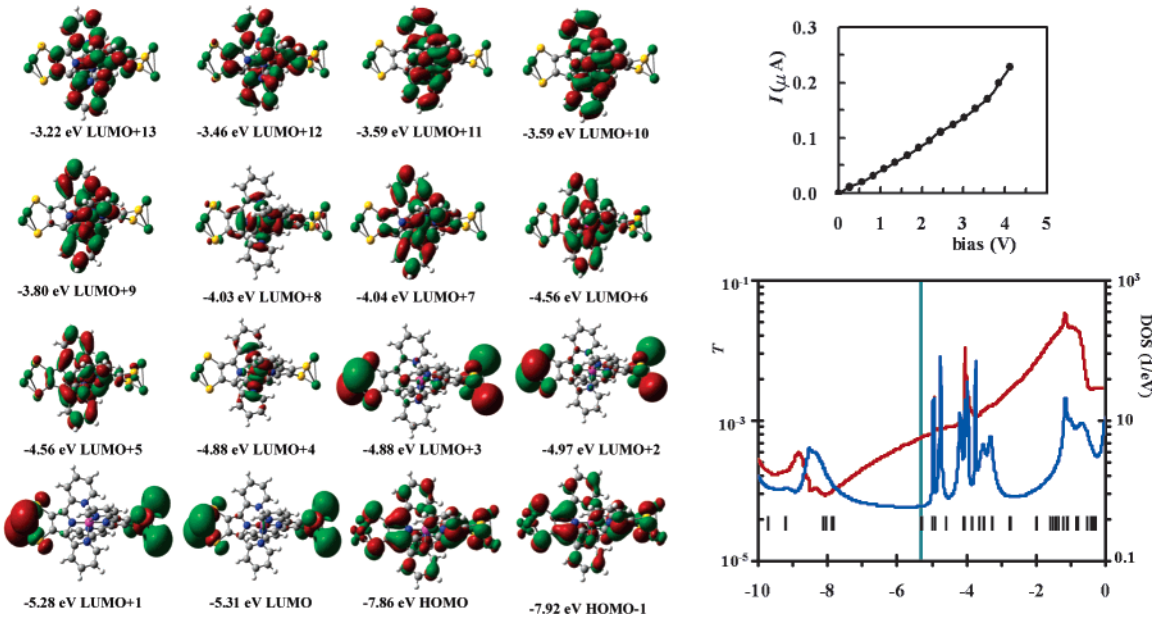

Figure 3. (left) Molecular orbital of the extended molecule (**4**) in the high oxidation state; (top right) $I-V$ characteristics; (bottom right) DOS (blue, right axis) and electron transmission probability (red, left axis) (the vertical green line represents the Au Fermi level, and the short black lines are electronic states of the extended molecule (**4**) in the high oxidation state).

energies, from −5.05 to −5.44 eV, are very close to the Fermi energy of Au at −5.31 eV (Figure 2). These delocalized MOs correspond to the peaks in the transmission probability curve in the vicinity of the Fermi level of the Au terminals. In the energy range −5.05 to −7 eV, besides these eight delocalized MOs, all other MOs are localized. The localized MOs have little contribution to the transmission probability. The unoccupied MOs (α-LUMO to α-LUMO+3 and β-LUMO to β-LUMO+3) are also localized and have little contribution to the transmission probability. The other delocalized MOs below −7 eV or above −2 eV do contribute to the transmission probability in their corresponding energy range. The transmission probability increases exponentially in the energy range −7 to 0 eV due to the increase in the energy of tunneling electrons.

From the energy of the occupied MOs that are close to the Fermi energy of the Au terminal, their delocalization characteristics, their contribution to the DOS, and the transmission probability, we can infer that hole conduction is the main mechanism of charge transport.

However, the shapes of MOs do not change much when the extended molecule (**4**) is in a high oxidation state (Figure 3). However, their energies are shifted to lower values; the lowest unoccupied MO (LUMO) has an energy of −5.31 eV, and the LUMO+1 to LUMO+13 have energies from −5.28 to −3.22 eV. The MOs correspond to the peaks in the DOS of the molecular device at a high oxidation state near the Fermi energy of the contact material Au (Figure 3).

The peaks from −4 to −3.5 eV in the electron transmission probability curve are mainly contributions from the delocalized LUMO+5 to LUMO+10. Their energies are close to the Fermi energy of the Au terminal; thus, their delocalization characteristics, their contribution to the DOS, and the transmission probability imply that electron conduction is from the cathode to the molecule. After the electron is injected into the molecule, the low oxidation state is formed and hole conduction takes place. Therefore, the conduction mechanism of the Co complex molecular device is hole conduction.

From Figures 2 and 3, we can find that the calculated $I-V$ characteristics of the Co complex are almost linear for both the low and high oxidation states. The high oxidation state has a higher conductance (∼0.04 μS) than the low oxidation state (∼0.02 μS). However, the total conductance contributed from each oxidation state must be the same; therefore, the molecular device stays in the low oxidation state two-thirds of the time and in the high oxidation state one-third of the time.

In summary, density functional theory calculations have been carried out to investigate the structure of the extended molecule (**4**). The calculation shows that the extended molecule has a D_{2d} symmetrical structure with two ligands perpendicular to each other and the Co atom locates at the center of a distorted octahedron formed by six donor N atoms. In the low oxidation state, the bond length between Co^{2+} and pyrrole nitrogen is much short than the bond length between Co^{2+} and pyridine nitrogen. The oxidation of Co^{2+} to Co^{3+} significantly shortens the bond length between Co and pyridine nitrogen.

The HOMO energy of the extended molecule is very close to the Fermi level of Au; this results in easy hole injection into the occupied MOs from the Au anode. However, the injection of a hole lowers the orbital energy and results in the LUMO energy being close to the Fermi level of Au. Thus, an electron is ready to be injected into the high oxidation state of the molecule from the Au cathode. Therefore, the Co complex is a good hole-conduction molecule.

Acknowledgment. This work has been supported by the DURINT and DURIP programs of the ARO and by the Moletronics and MoleApps programs of the DARPA/ONR and DARPA/AFOSR, respectively.

References and Notes

(1) Seminario, J. M.; Zacarias, A. G.; Tour, J. M. *J. Am. Chem. Soc.* **2000**, *122*, 3015−3020.

(2) Seminario, J. M.; Tour, J. M. Density Functional Theory for the Study of Single-Molecule Electronic Systems. In *Electron Correlations and Materials Properties*; Gonis, A., Kioussis, N., Ciftan, M., Eds.; Kluwer: New York, 1999.

(3) Chen, J.; Reed, M. A.; Asplund, C. L.; Cassell, A. M.; Myrick, M. L.; Rawlett, A. M.; Tour, J. M.; Van Patten, P. G. *Appl. Phys. Lett.* **1999**, *75*, 624−626.

(4) Reed, M. A. *Proc. IEEE* **1999**, *87*, 652−658.

(5) Allara, D. L.; Dunbar, T. D.; Weiss, P. S.; Bumm, L. A.; Cygam, M. T.; Tour, J. M.; Reinerth, W. A.; Yao, Y.; Kozaki, M.; Jones, L., II. *Ann. N.Y. Acad. Sci*. **1998**, *852*, 349−370.

(6) Seminario, J. M.; Zacarias, A. G.; Tour, J. M. *J. Am. Chem. Soc.* **1999**, *121*, 411−416.

(7) Tour, J. M.; Kosaki, M.; Seminario, J. M. *J. Am. Chem. Soc.* **1998**, *120*, 8486−8493.

(8) Seminario, J. M.; Cordova, L. E. *Proc. IEEE Nanotech. Conf.* **2001**, *1*, 146−150.

(9) Seminario, J. M.; Cordova, L. E.; Derosa, P. A. *Proc. IEEE* **2003**, *91*, 1958−1975.

(10) Tour, J. M.; Jones, L., II; Pearson, D. L.; Lamba, J. S.; Burgin, T. P.; Whitesides, G. W.; Allara, D. L.; Parikh, A. N.; Atre, S. *J. Am. Chem. Soc.* **1995**, *117*, 9529−9534.

(11) Reed, M. A.; Zhou, C.; Muller, C. J.; Burgin, T. P.; Tour, J. M. *Science* **1997**, *278*, 252−254.

(12) Zhou, C.; Deshpande, M. R.; Reed, M. A.; Jones, L., II; Tour, J. M. *Appl. Phys. Lett.* **1997**, *71*, 611−613.

(13) Yu, L. H.; Keane, Z. K.; Ciszek, J.; Chen, L.; Stewars, M. P.; Tour, J. M.; Natelson, D. *Phys. Rev. Lett.* **2004**, *93*, 266802.

(14) Sapp, S. A.; Elliott, C. M.; Contada, C.; Caramori, S.; Bignozzi, G. A. *J. Am. Chem. Soc.* **2002**, *124*, 11215−11222.

(15) Lay, P. A.; Mau, A. W. H.; Sasse, W. H. F.; Creaser, I. I.; Gahan, L. R.; Sargeson, A. M. *Inorg. Chem.* **1983**, *22*, 2347−2349.

(16) Park, J.; Pasupathy, A. N.; Goldsmith, J. I.; Chang, C.; Yaish, Y.; Petta, J. R.; Rinkoski, M.; Sethna, J. P.; Abruna, H. D.; McEuen, P. L.; Ralph, D. C. *Nature* **2002**, *417*, 722−725.

(17) Park, J.; Pasupathy, A. N.; Goldsmith, J. I.; Soldatov, A. V.; Chang, C.; Yaish, Y.; Sethna, J. P.; Abruna, H. D.; Ralph, d. C.; McEuen, P. L. *Thin Solid Films* **2003**, *438*−*439*, 457−461.

(18) Ren, X.; Alleyne, B. D.; Djurovich, P. I.; Adachi, C.; Tsyba, I.; Bau, R.; Thompson, M. E. *Inorg. Chem.* **2004**, *43*, 1697−1707.

(19) Derosa, P. A.; Seminario, J. M. *J. Phys. Chem. B* **2001**, *105*, 471−481.

(20) Seminario, J. M.; Zacarias, A. G.; Derosa, P. A. *J. Chem. Phys.* **2002**, *116*, 1671−1683.

(21) Kohn, W.; Sham, L. J. *Phys. Rev. A* **1965**, *140*, 1133−1138.

(22) Sham, L. J.; Kohn, W. *Phys. Rev.* **1966**, *145*, 561−567.

(23) Damle, P.; Ghosh, A. W.; Datta, S. *Chem. Phys.* **2002**, *281*, 171−187.

(24) Danielewicz, P. *Ann. Phys.* **1984**, *152*, 239−304.

(25) Caroli, C.; Combescot, R.; Nozieres, P.; Saint-James, D. *J. Phys. C* **1972**, *5*, 21−42.

(26) Datta, S. *Electronic Transport in Mesoscopic Systems*; Cambridge University Press: Cambridge, U.K., 1995.

(27) Landauer, R. *IBM J. Res. Dev.* **1957**, *1*, 223−231.

(28) Buttiker, M.; Imry, Y.; Landauer, R.; Pinhas, S. *Phys. Rev. B* **1985**, *31*, 6207−6215.

(29) Landauer, R. *Philos. Mag.* **1970**, *21*, 863−867.

(30) Hohenberg, P.; Kohn, W. *Phys. Rev. B* **1964**, *136*, 864−871.

(31) Frisch, M. J.; Trucks, G. W.; Schlegel, H. B.; Scuseria, G. E.; Robb, M. A.; Cheeseman, J. R.; Montgomery, J. A., Jr.; Vreven, T.; Kudin, K. N.; Burant, J. C.; Millam, J. M.; Iyengar, S. S.; Tomasi, J.; Barone, V.; Mennucci, B.; Cossi, M.; Scalmani, G.; Rega, N.; Petersson, G. A.; Nakatsuji, H.; Hada, M.; Ehara, M.; Toyota, K.; Fukuda, R.; Hasegawa, J.; Ishida, M.; Nakajima, T.; Honda, Y.; Kitao, O.; Nakai, H.; Klene, M.; Li, X.; Knox, J. E.; Hratchian, H. P.; Cross, J. B.; Bakken, V.; Adamo, C.; Jaramillo, J.; Gomperts, R.; Stratmann, R. E.; Yazyev, O.; Austin, A. J.; Cammi, R.; Pomelli, C.; Ochterski, J. W.; Ayala, P. Y.; Morokuma, K.; Voth, G. A.; Salvador, P.; Dannenberg, J. J.; Zakrzewski, V. G.; Dapprich, S.; Daniels, A. D.; Strain, M. C.; Farkas, O.; Malick, D. K.; Rabuck, A. D.; Raghavachari, K.; Foresman, J. B.; Ortiz, J. V.; Cui, Q.; Baboul, A. G.; Clifford, S.; Cioslowski, J.; Stefanov, B. B.; Liu, G.; Liashenko, A.; Piskorz, P.; Komaromi, I.; Martin, R. L.; Fox, D. J.; Keith, T.; Al-Laham, M. A.; Peng, C. Y.; Nanayakkara, A.; Challacombe, M.; Gill, P. M. W.; Johnson, B.; Chen, W.; Wong, M. W.; Gonzalez, C.; Pople, J. A. *Gaussian 03*, revision C.2; Gaussian, Inc.: Pittsburgh, PA, 2003.

(32) Becke, A. D. *J. Chem. Phys.* **1992**, *97*, 9173−9177.

(33) Perdew, J. P.; Wang, Y. *Phys. Rev. B* **1992**, *45*, 13244−13249.

(34) Perdew, J. P. Unified Theory of Exchange and Correlation beyond the Local Density Approximation. In *Electronic Structure of Solids*; Ziesche, P., Eschrig, H., Eds.; Akademie Verlag: Berlin, 1991; pp 11−20.

(35) Perdew, J. P.; Chevary, J. A.; Vosko, S. H.; Jackson, K. A.; Pederson, M. R.; Singh, D. J.; Fiolhais, C. *Phys. Rev. B* **1992**, *46*, 6671−6687.

(36) Hay, P. J.; Wadt, W. R. *J. Chem. Phys.* **1985**, *82*, 270−283.

(37) Hay, P. J.; Wadt, W. R. *J. Chem. Phys.* **1985**, *82*, 299−310.

(38) Wadt, W. R.; Hay, P. J. *J. Chem. Phys.* **1985**, *82*, 284−298.

(39) Petersson, G. A.; Bennett, A.; Tensfeldt, T. G.; Al-Laham, M. A.; Shirley, W. A.; Mantzaris, J. *J. Chem. Phys.* **1988**, *89*, 2193−2218.

(40) Petersson, G. A.; Al-Laham, M. A. *J. Chem. Phys.* **1991**, *94*, 6081−6090.

(41) Dolg, M.; Wedig, U.; Stoll, H.; Preuss, H. *J. Chem. Phys.* **1987**, *86*, 866−872.

(42) Schwerdtfeger, P.; Dolg, M.; Schwarz, W. H. E.; Bowmaker, G. A.; Boyd, P. D. W. *J. Chem. Phys.* **1989**, *91*, 1762−1774.

(43) Fuentealba, P.; Stoll, H.; von Szentpaly, L.; Schwerdtfeger, P.; Preuss, H. *J. Phys. B* **1983**, *16*, L323−L328.

(44) Andrae, D.; Haussermann, U.; Dolg, M.; Stoll, H.; Preuss, H. *Theor. Chim. Acta* **1990**, *78*, 247−266.

(45) Huheey, J. E.; Keiter, E. A.; Keiter, R. L. *Inorganic Chemistry*, 4th ed.; Harper Collins: New York, 1993.

(46) Roetti, C. The Crystal Code. In *Quantum-Mechanical Ab-initio Calculation of the properties of Crystalline Materials*; Pisani, C., Ed.; Springer-Verlag: Berlin, 1996; Vol. 67.

(47) Currie, M. T. *IEEE Int. Conf. Integrated Circuit Design Technol.* **2004**, 261−268.